

An extended finite element/level set method to study surface effects on the mechanical behavior and properties of nanomaterials

Mehdi Farsad¹, Franck J. Vernerey^{1,*},[†] and Harold S. Park²

¹*Department of Civil, Environmental and Architectural Engineering, University of Colorado at Boulder, Campus Box 428, Boulder, CO 80309-0428, U.S.A.*

²*Department of Mechanical Engineering, University of Colorado at Boulder, Boulder, CO 80309, U.S.A.*

SUMMARY

We present a new approach based on coupling the extended finite element method (XFEM) and level sets to study surface and interface effects on the mechanical behavior of nanostructures. The coupled XFEM-level set approach enables a continuum solution to nanomechanical boundary value problems in which discontinuities in both strain and displacement due to surfaces and interfaces are easily handled, while simultaneously accounting for critical nanoscale surface effects, including surface energy, stress, elasticity and interface decohesion. We validate the proposed approach by studying the surface-stress-driven relaxation of homogeneous and bi-layer nanoplates as well as the contribution from the surface elasticity to the effective stiffness of nanobeams. For each case, we compare the numerical results with new analytical solutions that we have derived for these simple problems; for the problem involving the surface-stress-driven relaxation of a homogeneous nanoplate, we further validate the proposed approach by comparing the results with those obtained from both fully atomistic simulations and previous multiscale calculations based upon the surface Cauchy–Born model. These numerical results show that the proposed method can be used to gain critical insights into how surface effects impact the mechanical behavior and properties of homogeneous and composite nanobeams under generalized mechanical deformation. Copyright © 2010 John Wiley & Sons, Ltd.

Received 9 October 2009; Revised 16 April 2010; Accepted 20 April 2010

KEY WORDS: surface elasticity; surface stress; nano-structure; XFEM; level set

INTRODUCTION

The recent progress in nanotechnology has led to the understanding that materials whose features reside at the nanometer length scales exhibit mechanical behavior and properties that

*Correspondence to: Franck J. Vernerey, Department of Civil, Environmental and Architectural Engineering, University of Colorado at Boulder, Campus Box 428, Boulder, CO 80309-0428, U.S.A.

[†]E-mail: franck.vernerey@colorado.edu

Contract/grant sponsor: NSF; contract/grant numbers: CMMI-0900607, CMMI-0750395

can differ considerably from those expected in the corresponding bulk material [1–4]. The main reason for these unique mechanical properties is due to nanoscale surface effects, which arise as surface atoms have fewer bonding neighbors than do their bulk counterparts. A scaling argument can then be presented in which these surface effects only become critical at nanometer length scales due to the relatively large surface area to volume ratio that is characteristic of nanomaterials [5–8].

The research that has gone into studying surface effects on the mechanical behavior and properties can be divided into three categories: theoretical, computational, and experimental. From a theoretical perspective, there has been a relative abundance of work to study surface effects on nanomaterials. The pioneering work in this area was performed by Gurtin and Murdoch, who devised a linear surface elastic model for nanostructures [9]. This work has formed the basis for future works, which have been performed by many authors, including Yang [10], Cammarata *et al.* [4], Streitz *et al.* [11], Miller and Shenoy [12], He *et al.* [13], Sharma *et al.* [1], Sun and Zhang [14] and Dingreville *et al.* [15].

Computationally, researchers have utilized both classical molecular dynamics (MD) and continuum finite element formulations based on the surface elasticity formulation of Gurtin and Murdoch to study surface effects on the mechanical behavior of nanomaterials. For example, Shenoy [5] used MD to evaluate the surface elastic properties of different FCC metals and discussed the importance of accounting for surface relaxation due to surface stress in calculating the surface elastic constants. Similarly, Mi *et al.* [6] used MD to calculate the elastic constants associated with various FCC metallic interfaces. It should be noted that the goal of both the Shenoy and Mi *et al.* works was to directly calculate using MD the surface elastic constants (surface stress and surface stiffness) that are needed for the surface elastic formulation of Gurtin and Murdoch.

A recent trend in computational mechanics is the notion of using finite element method (FEM)-based approaches to study surface effects on nanomaterials. The motivation for these FEM-based approaches is to avoid the intensive computational expense that arises from fully atomistic simulations, while simultaneously capturing the essential nanoscale surface effects. The most common approach has been to directly discretize the governing surface elastic equations of Gurtin and Murdoch; this has been done by Wei *et al.* [16], She *et al.* [17], and He *et al.* [18]. A similar approach to the one taken in the present work was done recently by Yvonnet *et al.* [19], who developed a computational technique combining the level set method and the extended finite element method (XFEM) to study surface effects on nanocomposites. However, the approach of Yvonnet *et al.* considered only weak discontinuities, i.e. the displacement across interfaces was assumed to be continuous, while only discontinuities in stress and strain across interfaces (or surfaces) was considered.

Alternatively, Park *et al.* [7, 20, 21] did not discretize the surface elastic equations of Gurtin and Murdoch, and instead presented an extension to the standard Cauchy–Born model called the surface Cauchy–Born (SCB) model in which surface energies were considered to capture nanoscale surface effects. The SCB model was recently utilized to study surface stress effects on the resonant frequencies (and thus elastic properties) of both FCC metal and silicon nanowires [22–24], and surface effects on the bending behavior of FCC metal nanowires [25].

This paper introduces a computational framework based on the theoretical development of Gurtin and Murdoch [26], XFEM and level sets to capture surface and interface effects on the mechanical behavior and properties of nanostructures. In particular, the presented method possesses

the following advantages:

- Owing to its continuum mechanics underpinnings, the method is computationally tractable and may be used to study surface and interface effects on nanostructures that have length scales, i.e. 10–100 nm, which are significantly larger than those that can be studied using fully atomistic techniques.
- The geometry of the structure is entirely defined by level set functions that are defined independently from the finite element mesh. Simple, regular FEM meshes may thus be used regardless of the geometric complexity of the nanostructure.
- The different elastic properties and constitutive response of nanoscale surfaces is described with a continuum description that naturally fits into the XFEM methodology. Thus, no special treatment is necessary to model jumps in stress, strain, and displacement arising due to free surfaces, interfaces or interface decohesion.
- The method is able to describe complex material behavior in nano-composites such as plasticity or damage. It thus presents a useful tool for studying surface and interface effects on the deformation and fracture of nano-composite structures.

The outline of the paper is as follows. We first describe the XFEM-level set formulation including the surface elasticity formulation of Gurtin and Murdoch. To validate the model, we study the surface-stress-driven relaxation of a fixed/free nanobeam, and compare the results with those obtained using both MD, and also the SCB model. Finally, we study the behavior of nanoplates under tension and bending, and compare the results with newly obtained analytic solutions. We demonstrate that the nanoscale surface effects are captured accurately, and demonstrate the length scales at which the surface effects can be expected to begin having a significant effect on the mechanical behavior and properties of nanomaterials.

CONTINUUM FORMULATION OF SOLIDS ACCOUNTING FOR SURFACE EFFECTS

Let us consider a two-dimensional (plane stress or plane strain) nano-structure in the x - y plane (Figure 1). In this figure, we denote each enclosed domain—that may represent the matrix domain and inclusion domains—by Ω_i so that $\Omega = \Omega_1 \cup \Omega_2 \cup \dots \cup \Omega_n$ where as Γ_i is the interface of region Ω_i . The outward unit vector for each region is also denoted by n_i . The displacement and traction boundary conditions, respectively, are $\partial\Omega_u$ and $\partial\Omega_f$. We now introduce the kinematics of the medium in the context of small deformations. Assuming that the bulk undergoes a smooth deformation, a material point belonging to Ω undergoes a displacement $\mathbf{u}(\mathbf{x})$. However, if one allows for interface decohesion, a jump in displacement may exist for a point on Γ such that $[\mathbf{u}](x) = u^+(x) - u^-(x)$, where $\mathbf{u}^+(\mathbf{x})$ and $\mathbf{u}^-(\mathbf{x})$ denote different sides of the interface. Following the work of Gurtin [26], we can introduce three strain measures ϵ , ϵ_s , and ϵ_d as follows:

$$\begin{aligned}\epsilon &= \frac{1}{2}(\nabla\mathbf{u} + \nabla\mathbf{u}^T) \quad \text{in } \Omega \\ \epsilon_s &= \mathbf{P} \cdot \epsilon \cdot \mathbf{P} \quad \text{on } \Gamma \\ \epsilon_d &= \mathbf{T} \cdot \epsilon_d^g \quad \text{on } \Gamma\end{aligned}\tag{1}$$

where ‘ \cdot ’ is used for the dot product. The quantity ϵ is the conventional small strain measure in the bulk, ϵ_s is the interface deformation. Furthermore, ϵ_d and ϵ_d^g are a measure of interface debonding

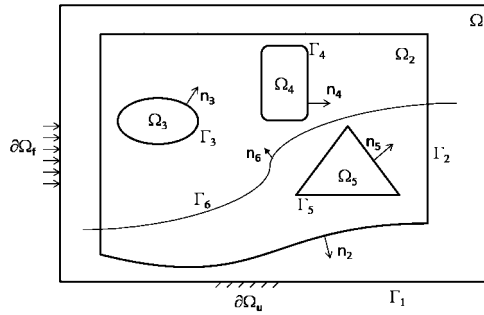


Figure 1. General outline of the nano-structure under study.

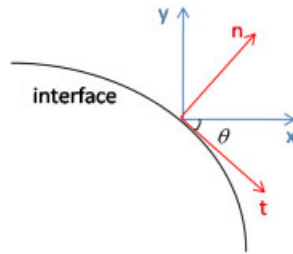


Figure 2. Local (t - n) and global (x - y) coordinates on a typical interface.

in local (normal and tangential directions to the interface) and global coordinates, respectively. These strain measures are defined as

$$\epsilon = \begin{bmatrix} \epsilon_{11} & \epsilon_{12} \\ \epsilon_{21} & \epsilon_{22} \end{bmatrix}, \quad \epsilon_s = \begin{bmatrix} \epsilon_{s11} & \epsilon_{s12} \\ \epsilon_{s21} & \epsilon_{s22} \end{bmatrix}, \quad \epsilon_d = \begin{bmatrix} \epsilon_t \\ \epsilon_n \end{bmatrix}, \quad \epsilon_d^g = \begin{bmatrix} \epsilon_1 \\ \epsilon_2 \end{bmatrix} \quad (2)$$

where t and n are local tangential and normal directions of the interface as shown in Figure 2. In Equation (1), \mathbf{P} is the tangential projection tensor to Γ and is defined by $\mathbf{P} = \mathbf{I} - \mathbf{n} \otimes \mathbf{n}$ (\mathbf{n} is normal to Γ), such that the components of the projections of a vector \mathbf{w} and a tensor \mathbf{W} on a surface of normal n are given by:

$$\mathbf{w}_s = \mathbf{P} \cdot \mathbf{w} \quad \text{and} \quad \mathbf{W}_s = \mathbf{P} \cdot \mathbf{W} \cdot \mathbf{P} \quad (3)$$

Furthermore, the transformation \mathbf{T} rotates the local tangential coordinate system associated with the interface to the global coordinate system. In other words, if $\mathbf{w}_{\text{local}}$ is a vector in the local coordinate system, this same vector $\mathbf{w}_{\text{global}}$ in the global coordinate system is written as:

$$\mathbf{w}_{\text{local}} = \mathbf{T} \cdot \mathbf{w}_{\text{global}} \quad (4)$$

From these definitions, we can introduce three stress measures, $\boldsymbol{\sigma}$, $\boldsymbol{\sigma}_s$, and $\boldsymbol{\sigma}_d$ as energy conjugate of ϵ , ϵ_s , and ϵ_d^g such that, following [26], the force balance for the nano-structure can be written

as follows:

$$\mathbf{div}\boldsymbol{\sigma} + \mathbf{b} = 0 \quad \text{in } \Omega \quad (5)$$

$$[\boldsymbol{\sigma} \cdot \mathbf{n}] + \mathbf{div}_s \boldsymbol{\sigma}_s = 0 \quad \text{on } \Gamma \quad (6)$$

$$\langle \boldsymbol{\sigma} \cdot \mathbf{n} \rangle - \boldsymbol{\sigma}_d = 0 \quad \text{on } \Gamma \quad (7)$$

In the above equation, we used the fact that $\mathbf{div}_s \boldsymbol{\sigma} = \nabla \boldsymbol{\sigma} : \mathbf{P}$, where ‘:’ is the double tensor contraction and the quantities \mathbf{b} , $[\boldsymbol{\sigma} \cdot \mathbf{n}]$, and $\langle \boldsymbol{\sigma} \cdot \mathbf{n} \rangle$ are the body force vector, jump, and average value of the traction field across the interface, respectively. Furthermore, the boundary conditions in Figure 1 are written in the standard form as

$$\begin{aligned} \boldsymbol{\sigma} \cdot \mathbf{n} &= -\mathbf{t} \quad \text{on } \partial\Omega_F \\ \mathbf{u} &= \mathbf{u}^* \quad \text{on } \partial\Omega_u \end{aligned} \quad (8)$$

where \mathbf{t} and \mathbf{u}^* are the inward traction and displacement, respectively. Using standard procedures [27] one may derive the weak form of the boundary value problem:

$$\begin{aligned} \text{find } \mathbf{u} \in \{\mathbf{u} \in H^1(\Omega_i) \text{ and } \mathbf{u} = \mathbf{u}^*, \delta\mathbf{u} = 0 \text{ on } \partial\Omega_u\} \\ \int_{\Omega} \boldsymbol{\sigma} : \delta\boldsymbol{\epsilon} \, d\Omega + \int_{\Gamma} \boldsymbol{\sigma}_s : \delta\boldsymbol{\epsilon}_s \, d\Gamma + \int_{\Gamma} \boldsymbol{\sigma}_d : \delta\boldsymbol{\epsilon}_d \, d\Gamma = \int_{\Omega} \mathbf{b} \cdot \delta\mathbf{u} \, d\Omega + \int_{\partial\Omega_F} \mathbf{t} \cdot \delta\mathbf{u} \, d\Gamma \end{aligned} \quad (9)$$

where we assumed that there are no applied external forces at the border of any open interface. To complete the model, a constitutive relation has to be introduced to describe the mechanical response of the composite under investigation. A variety of constitutive relations may be introduced to relate stress and strain measures, including plasticity and damage in the bulk and at the interface. In the present work, we restrict ourselves to the simple case of linear elasticity, which is valid for our assumption of small deformation. For the constitutive relation between surface stress and strain, in agreement with [4] and Shuttleworth’s equation we have:

$$\boldsymbol{\sigma}_s = \tau_0 \mathbf{I} + \frac{\partial \gamma}{\partial \boldsymbol{\epsilon}_s} \quad (10)$$

where τ_0 is the surface tension in the undeformed configuration, \mathbf{I} is surface unit tensor, and γ is surface energy coming from surface strain. Denoting $\boldsymbol{\sigma}_0 = \tau_0 \mathbf{I}$, Equation (10) and [26], the linear stress–strain relationship for our problem is written as

$$\boldsymbol{\sigma} = \mathbf{C} : \boldsymbol{\epsilon}, \quad \boldsymbol{\sigma}_s = \boldsymbol{\sigma}_0 + \mathbf{C}^s : \boldsymbol{\epsilon}_s, \quad \boldsymbol{\sigma}_d = \mathbf{C}^d : \boldsymbol{\epsilon}_d \quad (11)$$

where \mathbf{C} , \mathbf{C}^s are fourth-order tensors and show the elastic stiffness of the bulk and the interface tension, respectively. Also, \mathbf{C}^d denotes elastic stiffness of interface cohesion and is defined as

$$\mathbf{C}_{pq}^d = K_t \delta_{1p} \delta_{1q} + K_n \delta_{2p} \delta_{2q} \quad (12)$$

where K_t and K_n are cohesion constants in the directions t and n (Figure 2), respectively. \mathbf{C}^s will be defined in the next section considering surface elastic coefficients and the direction of surface normal vector. Finally, the isotropic elastic response of the bulk material is characterized by two

constants: the Young’s modulus E and the Poisson ratio ν . Substituting (11) into (9), one can reach the final weak form as

$$\int_{\Omega} \delta\epsilon : \mathbf{C} : \epsilon \, d\Omega + \int_{\Gamma} \delta\epsilon_s : \boldsymbol{\sigma}_0 \, d\Gamma + \int_{\Gamma} \delta\epsilon_s : \mathbf{C}^s : \epsilon_s \, d\Gamma + \int_{\Gamma} \delta\epsilon_d : \mathbf{C}^d : \epsilon_d \, d\Gamma$$

$$= \int_{\Omega} \delta\mathbf{u} \cdot \mathbf{b} \, d\Omega + \int_{\partial\Omega_F} \delta\mathbf{u} \cdot \mathbf{t} \, d\Gamma \tag{13}$$

or using the transformation matrix \mathbf{T} and tangential projection P defined in Equation (1), the weak form can finally be written in the compact form:

$$\delta W_b + \delta W_s + \delta W_d = \delta W_{\text{ext}} \tag{14}$$

where the bulk, surface, debonding, and external virtual energies $\delta W_b, \delta W_s, \delta W_d$ and δW_{ext} , respectively, are:

$$\delta W_b = \int_{\Omega} \delta\epsilon : \mathbf{C} : \epsilon \, d\Omega$$

$$\delta W_s = \int_{\Gamma} (\mathbf{P}\delta\epsilon\mathbf{P}) : \boldsymbol{\sigma}_0 \, d\Gamma + \int_{\Gamma} (\mathbf{P}\delta\epsilon\mathbf{P}) : \mathbf{C}^s : (\mathbf{P}\epsilon\mathbf{P}) \, d\Gamma$$

$$\delta W_d = \int_{\Gamma} (\mathbf{T} \cdot \delta\epsilon_d^g) : \mathbf{C}^d : (\mathbf{T} \cdot \epsilon_d^g) \, d\Gamma$$

$$\delta W_{\text{ext}} = \int_{\Omega} \delta\mathbf{u} \cdot \mathbf{b} \, d\Omega + \int_{\partial\Omega_F} \delta\mathbf{u} \cdot \mathbf{t} \, d\Gamma \tag{15}$$

AN XFEM/LEVELSET FORMULATION FOR NANO-STRUCTURES

The solution of Equations (1), (5) and (11) typically gives rise to discontinuities across the interface Γ . Indeed, the existence of surface tension is associated with a jump in strain across the interface (commonly called weak discontinuity), whereas the existence of a decohesion (through the cohesive law) leads to a jump in displacement across Γ (commonly called strong discontinuity). Many numerical techniques such as the FEM are developed for continuous field and fail to describe such discontinuities. To address this issue, the XFEM was first introduced to incorporate a jump in displacement occurring as a result of a propagating crack in a continuous medium [28, 29]. A key feature of this method resides in that the description of the discontinuity is independent of spatial discretization. Also, Belytschko *et al.* used XFEM in [30, 31] to define solids by implicit surfaces and also to modeling dislocations and interfaces. The method was further improved to model weak discontinuities, such as described in [32]. This method provides a natural platform on which Equations (1), (5) and (11) can be solved with great flexibility and minimal computational cost. In the present formulation, the displacement field $\tilde{\mathbf{u}}(\mathbf{x})$ is the sum of three terms (Equation (16)) parameterized by $\mathbf{u}, \bar{\mathbf{u}},$ and $\bar{\bar{\mathbf{u}}}$ that are associated with continuous, strong, and weak discontinuous fields, respectively, where last two terms do not have any kinematic interpretation. The approximation of the displacement in an element will then be written in the general form:

$$\tilde{\mathbf{u}}^e(\mathbf{x}) = \sum_{I=1}^n \mathbf{N}_I(\mathbf{x})\mathbf{u}_I + \sum_{J=1}^m \mathbf{N}_J(\mathbf{x})(H(\mathbf{x}) - H(\mathbf{x}_J))\bar{\mathbf{u}}_J + \sum_{J=1}^m \mathbf{N}_J(\mathbf{x})\chi_J(\mathbf{x})\bar{\bar{\mathbf{u}}}_J \tag{16}$$

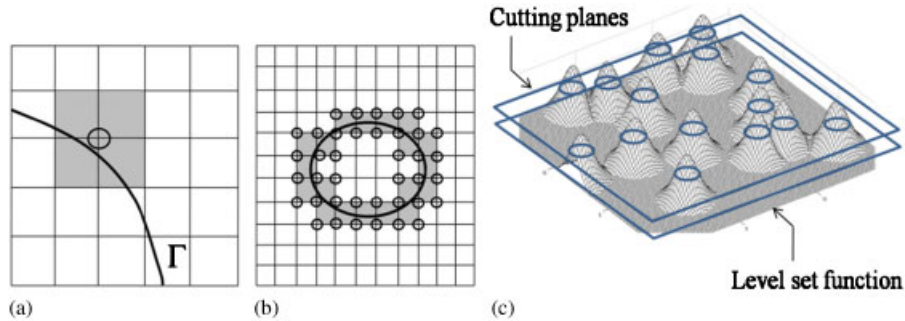


Figure 3. (a) Enriched node whose support is cut by the interface (zero level set); (b) enriched nodes and completely enriched elements for a closed interface; and (c) level set function and cutting plane to define circular inclusions in a square domain.

where

$$\mathbf{N}_I(\mathbf{x}) = \begin{bmatrix} N_I(\mathbf{x}) & 0 \\ 0 & N_I(\mathbf{x}) \end{bmatrix} \tag{17}$$

where the functions $N_I(\mathbf{x})$ are finite element shape functions associated with node I , $N_J(\mathbf{x})$ are the shape functions associated with the nodes of an element that has been cut by the interface (Figure 3(b)) and $H(\mathbf{x})$ and $\chi(\mathbf{x})$ are enrichment functions with the required discontinuities (ridge function and Heaviside function, respectively [32, 33]). In Equation (16), n is the total number of nodes per element, whereas m is the number of enriched nodes ($m \leq n$). By definition, an enriched node belongs to an element that is cut by the interface as depicted in Figure 3. To define the geometry of interface in a general fashion, we introduce a level set function $\phi(\mathbf{x})$ such that the interface is defined by the intersection of that a cutting plane, as depicted in Figure 3(c). With this description, the sign of ϕ is opposite in two sides of discontinuity. An attractive feature of using level sets is that the unit normal vector \mathbf{n} to the interface is determined by the gradient of the function $\phi(x)$ as follows:

$$\mathbf{n}(\mathbf{x}) = \frac{\nabla \phi(x)}{\|\nabla \phi(x)\|} \tag{18}$$

Let us now focus on the Heaviside and ridge functions appearing in (16). Referring to Figure 4, the Heaviside function makes a jump in displacement (strong discontinuity); in contrast, a ridge function causes a jump in strain field (weak discontinuity) across the interface that is related to derivative of displacement. Without going into details, the Heaviside and ridge functions are defined by (in one dimension):

$$H(\phi) = \begin{cases} 1, & \phi > 0 \\ 0, & \phi < 0 \end{cases} \quad \text{and} \quad \chi_j(\mathbf{x}) = |\phi(\mathbf{x})| - |\phi(\mathbf{x}_j)| \tag{19}$$

The finite element equations governing the deformation of nano-composites is now derived by substituting the displacement approximation $\tilde{\mathbf{u}}^e$ from (16) into the weak form given in (14) and (15). For this, stress, strain, and elasticity matrices are first rewritten in Voigt notation [27].

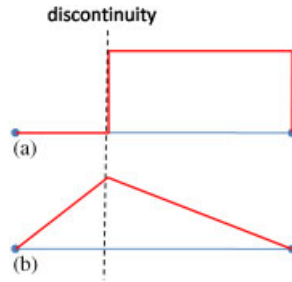


Figure 4. A general form of (a) Heaviside and (b) ridge functions to define strong and weak discontinuities, respectively.

Bulk energy

Starting with the bulk energy, the finite element approximation $\delta\tilde{W}_b^e$ of δW_b^e gives rise to the standard expression:

$$\delta\tilde{W}_b^e = \int_{\Omega} \delta\epsilon^e : \mathbf{C}^e : \epsilon^e d\Omega = \delta\mathbf{u}^{eT} \cdot \left(\int_{\Omega} \mathbf{B}^{eT} \{ \mathbf{C}^e \} \mathbf{B}^e d\Omega \right) \cdot \mathbf{u}^e \tag{20}$$

where \mathbf{C}^e and $\{ \mathbf{C}^e \}$ are bulk constitutive relation matrix for element e in tensorial and Voigt notations, respectively. In addition, the standard \mathbf{B} matrix is written in terms of the shape functions \bar{N} as follows:

$$\mathbf{B}^e = [\mathbf{B}_1^e \ \mathbf{B}_2^e \ \dots \ \mathbf{B}_{n+m}^e] \quad \text{and} \quad \mathbf{B}_I^e = \begin{bmatrix} \frac{\partial \bar{N}_I(\mathbf{x})}{\partial x_1} & 0 \\ 0 & \frac{\partial \bar{N}_I(\mathbf{x})}{\partial x_2} \\ \frac{\partial \bar{N}_I(\mathbf{x})}{\partial x_2} & \frac{\partial \bar{N}_I(\mathbf{x})}{\partial x_1} \end{bmatrix} \tag{21}$$

In the above equation, n and m are the number of nodes and enriched nodes of element e , respectively and N is the finite element shape function; $\bar{N}(\mathbf{x})$ equals $N(\mathbf{x})$, $H(\mathbf{x}) \times N(\mathbf{x})$, and $\chi(\mathbf{x}) \times N(\mathbf{x})$ for a normal FEM, strong discontinuity, and weak discontinuity degree of freedom, respectively; where, $H(\mathbf{x})$ and $\chi(\mathbf{x})$ are Heaviside and ridge functions, respectively.

Surface energy

The contribution $\delta\tilde{W}_s^e$ from the surface energy in element e is now derived. Using expression (16) for \mathbf{u} in an element, one can show that:

$$\begin{aligned} \delta\tilde{W}_s^e &= \int_{\Gamma} (\mathbf{P} \delta \epsilon \mathbf{P}) : \boldsymbol{\sigma}_0 d\Gamma + \int_{\Gamma} (\mathbf{P} \delta \epsilon \mathbf{P}) : \mathbf{C}^s : (\mathbf{P} \epsilon \mathbf{P}) d\Gamma \\ &= \delta\mathbf{u}^{eT} \left(\int_{\Gamma} \mathbf{B}^{eT} \mathbf{M}_P^T \cdot \{ \boldsymbol{\sigma}_0 \} d\Gamma + \int_{\Gamma} \mathbf{B}^{eT} \mathbf{M}_P^T \cdot \{ \mathbf{C}^s \} \cdot \mathbf{M}_P \mathbf{B}^e d\Gamma \right) \mathbf{u}^e \end{aligned} \tag{22}$$

where $\{\sigma_0\}$ and $\{C^s\}$ are expressions of the surface tension σ_0 and surface stiffness C^s in Voigt notation. The matrix \mathbf{M}_p gives the relationship between surface strain ϵ_s and the bulk strain ϵ so that $\epsilon_s = \mathbf{M}_p \epsilon$ [19, 26] and takes the form:

$$\mathbf{M}_p = \begin{bmatrix} P_{11}^2 & P_{12}^2 & P_{11}P_{12} \\ P_{12}^2 & P_{22}^2 & P_{22}P_{12} \\ 2P_{11}P_{12} & 2P_{22}P_{12} & P_{12}^2 + P_{11}P_{22} \end{bmatrix} \quad (23)$$

Following MD simulations of nanomaterials (such as [1, 2, 5, 6]), one can build the surface elastic coefficients matrix \mathbf{S}^s as

$$\mathbf{S}^s = \begin{bmatrix} S_{1111} & S_{1122} & 0 \\ S_{1122} & S_{2222} & 0 \\ 0 & 0 & S_{1212} \end{bmatrix} \quad (24)$$

where 1 and 2 stand for (100) and (110) directions, respectively. Consequently, for the nano metals under study, the surface tension constitutive matrix is defined as:

$$\{C^s\} = \mathbf{M}_p^T \mathbf{S}^s \mathbf{M}_p \quad (25)$$

Debonding energy

Following [33] and Equations (16) and (19), one can write the amount of jump in displacement across the interface in global coordinate for an element as

$$[\mathbf{u}^h(\mathbf{x})] = \sum_{J=1}^m \mathbf{N}_J^e(\mathbf{x}) \bar{\mathbf{u}}_J^e \quad (26)$$

where \mathbf{N}_J and $\bar{\mathbf{u}}_J$ are the same variables as in Equation (16) and m is the number of enriched nodes in element e . Using Equation (26), we can reach the global debonding strain measure as:

$$\epsilon_d^g = \sum_{J=1}^m \mathbb{B}_J^e(x) \bar{\mathbf{u}}_J^e \quad \text{where} \quad \mathbb{B}_J^e = \begin{bmatrix} \frac{\partial N_J^e}{\partial x} & 0 \\ 0 & \frac{\partial N_J^e}{\partial y} \end{bmatrix} \quad (27)$$

By substituting Equation (27) into (15), one can write the internal energy corresponding with debonding for one element as:

$$\delta \tilde{W}_d^e = \int_{\Gamma} (\mathbf{T} \cdot \delta \epsilon_d) : \mathbf{C}^d : (\mathbf{T} \cdot \epsilon_d) d\Gamma \quad (28)$$

$$= \delta \bar{\mathbf{u}}^e T \cdot \left(\int_{\Gamma} \mathbb{B}^{eT} \mathbf{T}^T \mathbf{C}^d \mathbf{T} \mathbb{B}^e d\Gamma \right) \cdot \bar{\mathbf{u}}^e \quad (29)$$

External energy

Finally, the finite element approximation of the external energy is only associated with standard shape functions, and is given by:

$$\delta \tilde{W}_{\text{ext}}^e = \delta \mathbf{u}^{eT} \cdot \left(\int_{\Omega} \mathbf{N}^{eT} \mathbf{b} \, d\Omega + \int_{\partial\Omega_F} \mathbf{N}^{eT} \mathbf{t} \, d\Gamma \right) \quad (30)$$

Final XFEM equation

Using Equations (20), (22), (28), and (30), and the weak form in (14) and (15), the XFEM equation for one element finally takes the form:

$$(\mathbf{K}_b^e + \mathbf{K}_d^e + \mathbf{K}_s^e) \cdot \mathbf{d}^e = \mathbf{f}_{\text{ext}}^e - \mathbf{f}_s^e \quad (31)$$

where the nodal displacement \mathbf{d}^e is comprised of contributions from the continuous, weakly discontinuous, and strongly discontinuous fields:

$$\mathbf{d}^e = [\mathbf{u} \quad \bar{\mathbf{u}} \quad \bar{\bar{\mathbf{u}}}]^T \quad (32)$$

the tangent matrices for the bulk, surface energy, and debonding contributions are, respectively:

$$\mathbf{K}_b^e = \int_{\Gamma} \mathbf{B}^{eT} \{ \mathbf{C}^e \} \mathbf{B}^e \, d\Gamma \quad (33)$$

$$\mathbf{K}_s^e = \int_{\Gamma} \mathbf{B}^{eT} \mathbf{M}_p^T \{ \mathbf{C}^s \} \mathbf{M}_p \mathbf{B}^e \, d\Gamma \quad (34)$$

$$\mathbf{K}_d^e = \int_{\Gamma} \mathbb{B}^{eT} \mathbf{T}^T \mathbf{C}^d \mathbf{T} \mathbb{B}^e \, d\Gamma \quad (35)$$

and the surface tension and external force vectors are:

$$\mathbf{f}_s^e = \int_{\Gamma} \mathbf{B}^{eT} \mathbf{M}_p^T \cdot \{ \boldsymbol{\sigma}_0 \} \, d\Gamma \quad (36)$$

$$\mathbf{f}_{\text{ext}}^e = \int_{\Omega} \mathbf{N}^{eT} \mathbf{b} \, d\Omega + \int_{\partial\Omega_F} \mathbf{N}^{eT} \mathbf{t} \, d\Gamma \quad (37)$$

A significant advantage in using the above formulation in the study of composite materials with complex shapes (Figure 1) is that a structured finite element mesh can be introduced independently from internal and external boundaries. Instead, a level set function will be introduced on top of the XFEM mesh to describe material interfaces that can be associated with strong and weak discontinuities. In particular, free boundaries do not need to conform to the FEM mesh but can be described as an interface that is totally disconnected from the external region. This will be done by enforcing a strong discontinuity to describe the displacement jump on the boundary. This feature is very attractive and in fact necessary to model the elasticity of free surfaces in nano-materials, as illustrated in the next examples. Referring to Figure 1, one distinguishes two regions, an internal region Ω_2 representing the medium under study and an external region Ω_1 that plays no role in the problem solution. Two strategies may thus be considered to solve this problem. In the first strategy, one may consider the region Ω_1 as a material with negligible stiffness, whose displacement is

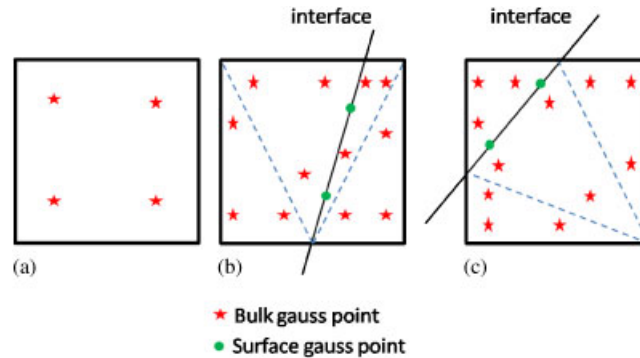


Figure 5. Typical gauss points: (a) normal element; (b) and (c) enriched elements.

continuous across γ . This method does not require the existence of a strong discontinuity, but suffers from the fact that it leads to an ill-conditioned global stiffness matrix (due to the small or vanishing stiffness). The second strategy, which is described in this paper, overcome this issue by considering a finite material stiffness in the external region, together with the existence of a displacement discontinuity across the free boundary. The strong discontinuity ensures that the displacement fields in the two regions are completely independent, and thus that the material in Ω_2 does not influence the solution. This strategy therefore relies on the introduction of both a strong and weak discontinuity (to describe surface elasticity) on the interface.

In this paper, bilinear four node quadrilateral elements are used. Furthermore, for integrating purposes, four Gauss points are considered in normal and partially enriched elements. In addition, following [34], sub-triangles are used on both sides of an interface in an enriched element. This method allows to define enough Gauss points to perform the integration in the enriched region; finally, the integration on surfaces is performed under the assumption that the interface consists of a straight line on which we use two gauss points. Figure 5 shows the gauss points and sub-triangles used in different situations.

NUMERICAL EXAMPLES

In order to illustrate the aforementioned model and for validation purposes, we investigate the mechanical properties of five relevant nanostructures and compare the numerical results with the analytical solutions. In particular, we concentrate on the following problems:

- The strain relaxation of nanoplates subjected to surface stress on its boundaries. We investigate two cases: a homogeneous plate and a composite bilayered plate.
- The effects of surface elasticity on the axial stiffness of nanoplates (both in uniaxial deformation and bending).
- The effect of the combination of surface decohesion and surface elasticity on the overall mechanical response of a plate with an inclusion.

For each problem, material interfaces (including the boundary of the structure) are modeled using both strong and weak discontinuities. The strong discontinuity allows the structure under study to

Table I. S_{ijkl} (surface stiffness), E (bulk Young's modulus), and ν (Poisson ratio) for Au, Pt and Ni from atomistic calculations [6].

Material	E (GPa)	ν	$S_{1111}=S_{2222}$ (J/m ²)	$S_{1122}=S_{2211}$ (J/m ²)	S_{1212} (J/m ²)	τ^0 (J/m ²)
Au	36	0.44	5.26	2.53	3.95	1.57
1(Pt)	200	0.38	13.25	9.30	5.12	2.52
2(Ni)	168	0.31	6.23	-4.72	0.93	1.37
$\frac{1}{2}$	—	—	9.34	-1.98	-4.94	0.34

deform independently from the surrounding medium, i.e. such that free surfaces are present on the boundary of the nanostructure, while the weak discontinuity permits the description of stress/strain discontinuity typically arising when a surface stress is present. All analysis are performed in two-dimensional plane strain conditions, valid for plates whose depth are large in comparison with their length and thickness. In this context, the plates are represented by a rectangular domain, discretized with 50 4-node quadrilateral elements in the length direction, and 20 4-node quadrilateral elements in the thickness direction, respectively. In terms of materials, we concentrate on three cases: gold (Au), platinum (Pt), and nickel (Ni), whose surface properties are obtained from MD analyses performed in [6] and shown in Table I.

Surface-stress-driven relaxation of a nanoplate

The first example we present focuses on validating the proposed XFEM/level set formulation as compared with a benchmark atomistic calculation. The specific problem we consider is illustrated in Figure 6, which demonstrates a fixed/free gold nanoplate of length $L=25$ nm, with thickness $t=10$ nm, and infinite width w to mimic plane strain conditions. In this example, due to the existence of tensile surface stresses, the gold nanoplate will undergo compressive axial strains. The key point we wish to demonstrate, for the first time, is that the surface elastic formulation of Gurtin and Murdoch is capable of capturing the surface-stress-driven axial relaxation. By noting that the surface energy (force per unit length) on the nanoplate equals τ^0 , while the resulting axial stress in the nanoplate is σ , we can state from equilibrium considerations along the axial direction of the nanoplate that

$$\sigma wt = 2w\tau^0 + 2t\tau^0 = 2\tau^0(w+t) \quad (38)$$

Because $w \gg t$, we can neglect t in the right-hand side of Equation (38), giving:

$$\sigma = \frac{2\tau^0}{t} \quad (39)$$

Finally, if the bulk Young's modulus is E , the axial strain in bulk due to surface-stress-induced compression can be written as:

$$\varepsilon = \frac{2\tau^0}{Et} \quad (40)$$

For the material properties of gold in Table I, Equation (40) gives an axial compressive strain of 0.00872 in the nanoplate due to surface stresses. Furthermore, Figure 7 shows a comparison for axial strain between Equation (40) and XFEM. As can be seen, when points along the axial direction of the nanoplate that are far from the free end are considered, the theoretical results

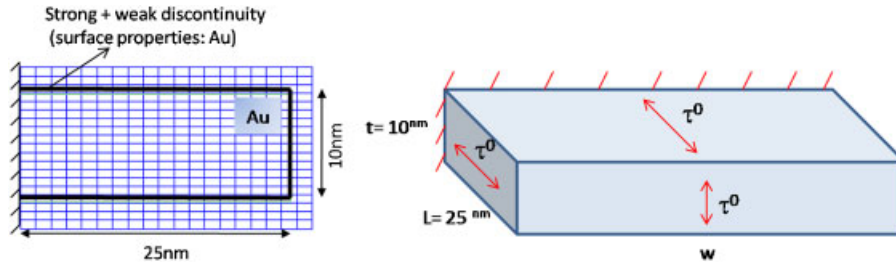


Figure 6. Schematic of a gold nanoplate, and the resulting XFEM discretization.

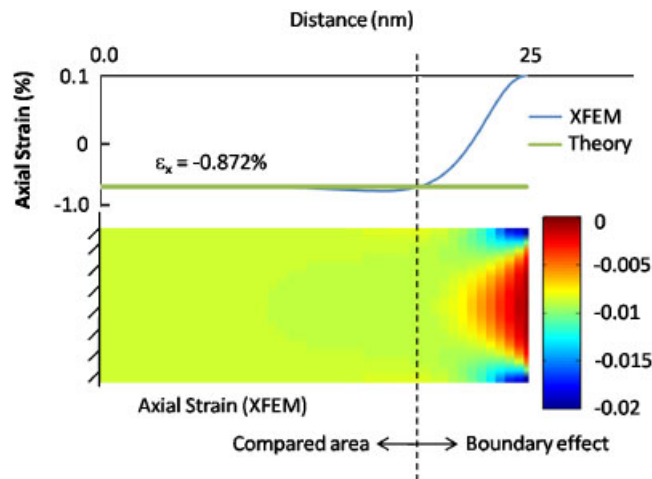


Figure 7. A comparison of surface-stress-driven compressive axial strain as computed using Equation (40) and XFEM along the gold nanoplate length.

from Equation (40) and the XFEM simulations match exactly. We note that in Equation (40), we have neglected the effects of Poisson ratio, surface elastic constants and boundary conditions; because of this, the Poisson ratio and surface elastic constants have been set to zero in the XFEM calculations.

To further validate the XFEM results, we compare them to results previously obtained by Park and Klein [7] for the surface-stress-driven relaxation of a gold nanoplate obtained using both molecular statics (MS) simulations using an embedded atom (EAM) potential for gold, and the SCB model of Park and Klein [7]. For the MS simulation, a $25 \times 10 \times 80$ nm fixed/free gold nanoplate consisting of 1.25 million atoms was considered, with periodic boundary conditions along the 80 nm direction to mimic infinite plane strain conditions. For the SCB calculations, the same $25 \times 10 \times 80$ nanoplate was considered, with no periodic boundary conditions; the 80-nm width was chosen to mimic a very wide nanoplate. Twenty thousand 8-node hexahedral elements were used to discretize the nanoplate for the SCB calculations. Both the MS and SCB calculations used EAM potentials for gold, which are the basis for the material properties for gold shown in Table I.

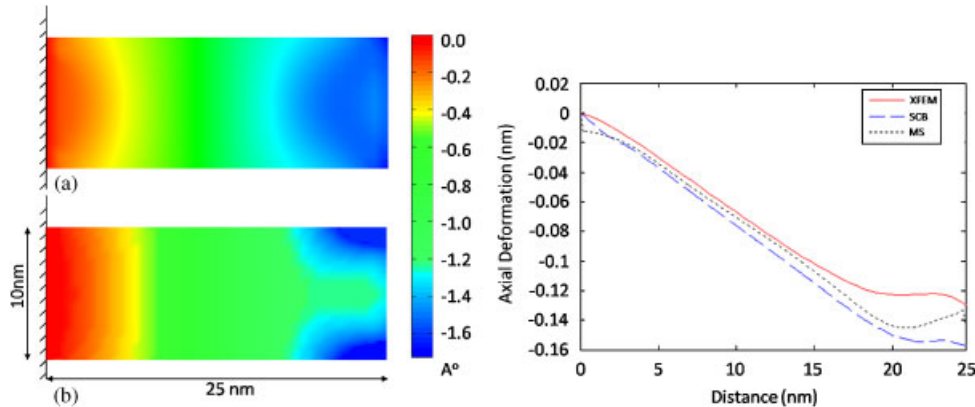


Figure 8. Surface-stress-driven axial compressive displacement profile from (a) XFEM and (b) SCB calculations. (Right) Surface-stress-driven axial compressive displacement from the fixed end of the nanoplate for XFEM, SCB and MS simulations.

Figure 8 shows the change in axial displacement versus distance from the fixed end for the XFEM, MS, and SCB calculations. We first note that the XFEM results are qualitatively similar to the SCB and MS results, in particular showing an essentially linear compressive displacement moving away from the fixed end, with a decrease in compressive displacement once the free surface is reached. We additionally note that the XFEM solution underestimates the compressive displacement along the nanoplate, whereas the SCB solution overestimates the compressive displacement. The SCB solution overestimates the compressive displacement because, as discussed by Park and Klein [7], the homogeneous deformation assumption that is enforced by using the Cauchy–Born hypothesis restricts deformation of the surface atoms, which thus results in the surface atoms having a larger surface stress at equilibrium as compared with the MS calculation. In contrast, the XFEM calculation underestimates the MS solution because the surface stress and surface elastic constants that are used in the XFEM calculation are constant, and furthermore are equilibrated values as they represent values taken from atomistic simulations in which the effects of surface relaxation have been accounted for [5]. Because of this, the surface effects in the XFEM calculation are smaller than in the MS simulation, and thus the XFEM displacements due to surface stresses are smaller than are observed in the MS simulation.

Surface effects on the axial stiffness of a nanoplate

In the previous example, the XFEM results were shown to be independent of the surface elastic constants. Because of this, and to verify and demonstrate the effect of surface elastic constants, we consider the same nanoplate as shown in Figure 6, although with length $L = 100$ nm. In addition, we impose an applied axial force F on the plate. Because of this, we expect that both the bulk and surface elastic constants will be needed to resist the tensile deformation due to the applied axial force. If we consider σ and τ as the axial stresses in the bulk and surface energy (force per unit length) of the nanoplate, respectively, we can write:

$$F = \sigma(wt) + \tau[2(w+t)] \quad (41)$$

Because $w \gg t$, we can neglect t in the $w + t$ term in (41) and write as:

$$\frac{F}{w} = \sigma t + 2\tau \quad (42)$$

If E and S_{1111} are the bulk Young's modulus and axial surface elastic constant, respectively, we can write that:

$$\varepsilon_1 = \frac{\sigma}{E} \quad \text{and} \quad \varepsilon_2 = \frac{\tau}{S_{1111}} \quad (43)$$

where ε_1 and ε_2 are the axial strains in the bulk and surface, respectively. Combining Equations (42) and (43) and noting that $\varepsilon_1 = \varepsilon_2 = \delta L/L$, we obtain:

$$\frac{F/w}{\delta L} = \frac{Et}{L} + \frac{2S_{1111}}{L} = K_b + K_s \quad (44)$$

where K_b and K_s are the bulk and surface axial stiffness, respectively. From (44), we note that if material properties for gold as previously shown in Table I are considered, because the bulk Young's modulus E is much greater than S_{1111} , we expect that the surface stiffness K_s will be negligible for large plates, while becoming increasingly important for smaller nanoplates. Furthermore, Equation (44) demonstrates that the aspect ratio of the plate t/L will have a significant effect on the bulk, and thus total stiffness of the nanoplate. Figure 9 shows the change in axial stiffness as a function of the nanoplate length, where the nanoplate aspect ratio t/L was kept constant at 10. As can be seen in Figure 9, an excellent agreement is found between the theoretical solution in Equation (44) and the XFEM solution. We also note that Figure 9 demonstrates the logical finding that a positive surface elastic coefficient S_{1111} , i.e. that would occur for most FCC metals, leads to an additional resistance against deformation (axial or flexural) of the surface. When the surface area to volume ratio becomes large enough, i.e. as the length of the nanoplate becomes smaller than 1000 nm in Figure 9, the resistance due to the positive surface elastic constant manifests itself in the form of an overall increase in axial stiffness for the nanoplate.

Surface and interface stress-driven relaxation of a bi-layered nanoplate

In our third numerical example, we seek to demonstrate the capabilities of the proposed XFEM-level set approach in capturing not only surface stress effects, but also interface stress effects due to a bi-material interface. Referring to Figure 10, we consider a fixed/free bi-layered Pt/Ni nanoplate, with material properties for Pt, Ni and the Pt/Ni interface shown in Table I. To emphasize on the effect of surface tension alone, the surface stiffness is neglected in this example. This will permit to derive a simple analytical solution that can be compared with our numerical results.

If we consider w and t as the width and depth of the nanoplate, respectively, and if the depth of each material (1 and 2) is $t/2$, for the equivalent section that is built of material 1, we can calculate x (the neutral axis distance from the top end of section) so that:

$$w \frac{3t}{4} \frac{t}{2} + nw \frac{t}{2} \frac{t}{4} = x(w + nw) \frac{t}{2} \quad (45)$$

where $n = E_2/E_1$ and E_1 and E_2 are the Young's modulus of material 1 and 2, respectively. Finally, x can be calculated from Equation (45) as:

$$x = \frac{t(3+n)}{4(1+n)} \quad (46)$$

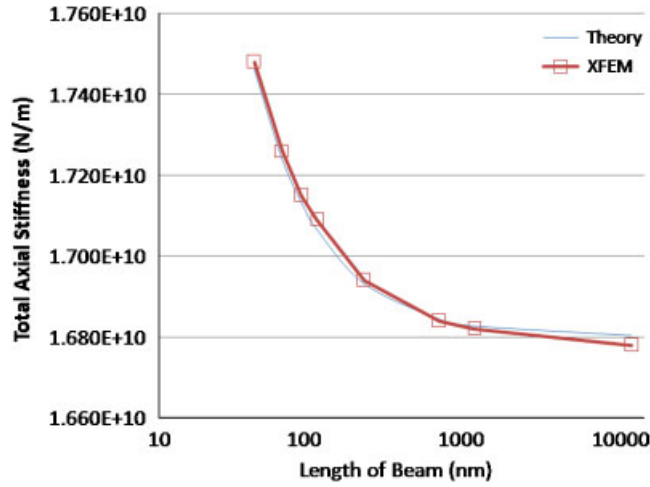


Figure 9. Surface effects on the size-dependent axial stiffness of a gold nanoplate with a constant aspect ratio of 10.

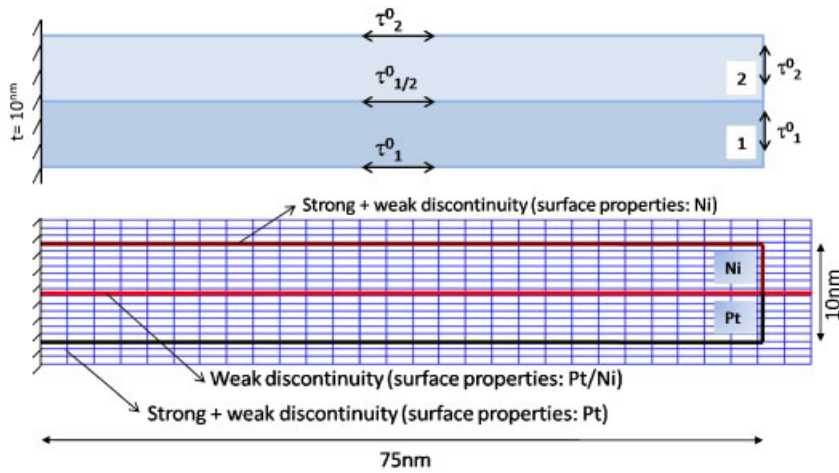


Figure 10. General outline of fixed/free bi-layered nano-beam including both surface and interface effects.

If we define τ_1^0 , τ_2^0 , and τ_{12}^0 as the surface energy (force per unit length) on materials 1, 2 and the interface of materials 1 and 2, respectively, we can calculate the induced moment (M) in the section that results from the material and surface elastic property differences between materials 1 and 2 as:

$$M = (\tau_1^0 w)(t - x) - (\tau_2^0 w)x + (\tau_{12}^0 w) \left(\frac{t}{2} - x \right) \tag{47}$$

Defining I and ρ as the moment of inertia and the equivalent radius of curvature respectively, i.e.:

$$\frac{1}{\rho} = \frac{M}{E_1 I} \quad \text{and} \quad \varepsilon_1 = \frac{y}{\rho} \quad (48)$$

where y and ε_1 are the distance from the neutral axis and the axial strain due to the moment M respectively, we find that:

$$\varepsilon_1 = \frac{\tau_1^0(t-x) - \tau_2^0 x + \tau_{12}^0 \left(\frac{t}{2} - x\right)}{\left(\frac{1}{12} \left(\frac{t}{2}\right)^3 (n+1) + \left(\frac{t}{2}\right) \left[\left(\frac{3t}{4} - x\right)^2 + n \left(x - \frac{t}{4}\right)^2 \right]\right) E_1} \quad (49)$$

To calculate the axial strain that comes from surface-stress-driven relaxation (ε_2), and using the same method used for homogeneous nanoplate, we find that:

$$\varepsilon_2 = \frac{\tau_1^0 + \tau_2^0 + \tau_{12}^0}{E_1 \frac{t}{2} (1+n)} \quad (50)$$

Finally, the total axial strain due to surface and interface stresses can be written as:

$$\varepsilon = \varepsilon_1 + \varepsilon_2 \quad (51)$$

Considering a fixed/free nanoplate, we can calculate the deflection δ of the nanoplate to be

$$\delta = \frac{1}{2\rho} x^2 \quad (52)$$

where x is the distance from the fixed end of the beam and ρ can be calculated from Equation (48). We first show in Figure 11(a) the deformed configuration of the bi-layered nanoplate, as well as a comparison of the surface and interface stress-induced axial strain as calculated using both XFEM and the analytic solution given in Equations (49)–(51). We additionally show in Figure 11(b) a comparison between XFEM and the analytic solution for the transverse deflection of the bi-layered nanoplate. In both cases, excellent agreement between XFEM and the analytic solution is observed. Another interesting point to discuss is the fact that the bi-layered plate deflects downward, as shown in Figures 11(a) and (b). This occurs because the surface stress for the bottom (Pt) surface of the plate is larger than the surface stress on the top (Ni) surface of the nanoplate.

Surface effects on the size-dependent bending stiffness of a nanobeam

For the final numerical example, we consider surface effects on the size-dependent bending stiffness of a nanobeam, where the problem schematic is illustrated in Figure 12. The material we use in this example is gold (Au) whose properties are mentioned in Table I. For this problem, we consider that the nanobeam has fixed/fixed boundary conditions, and is motivated by recent experimental findings [35, 36] that have shown that the bending stiffness of FCC metal nanowires increases dramatically with decreasing nanowire diameter. Before showing the XFEM results, we first derive

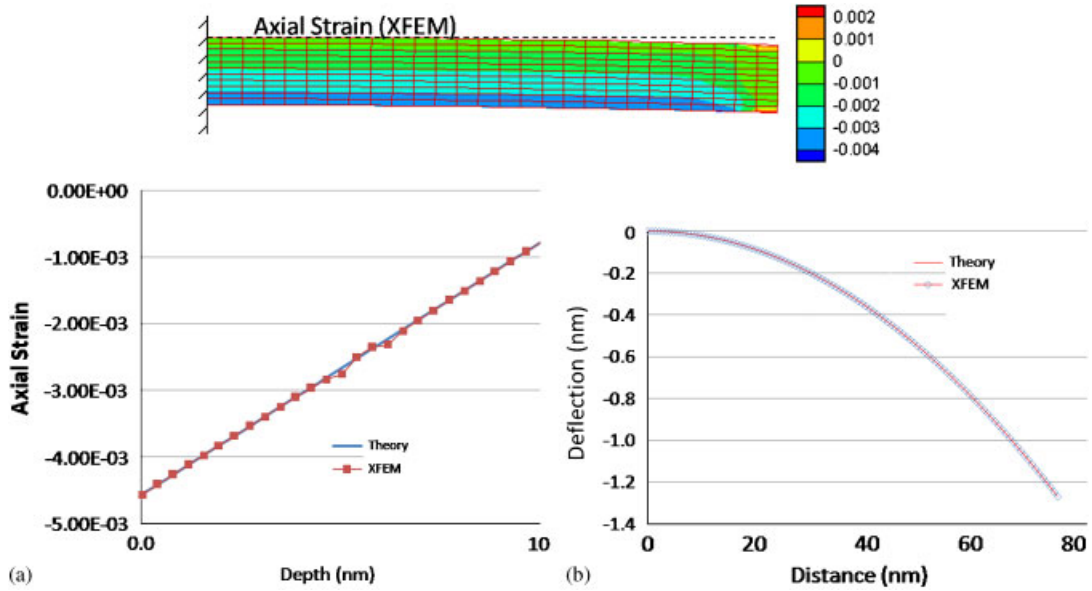


Figure 11. (a) Axial strain comparison between XFEM and theory (Equations (49)–(51)) due to both surface and interface stress for a bi-layered Pt/Ni nanoplate, (b) transverse deflection comparison along a bi-layered Pt/Ni nanoplate between XFEM and theory (Equation (52)) due to both surface and interface stress.

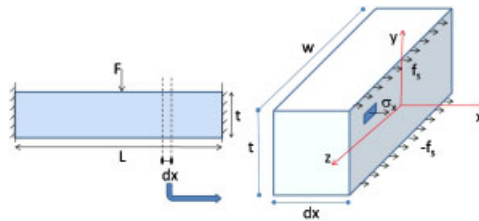


Figure 12. Schematic of a fixed–fixed nanobeam bent by an applied force F .

a theoretical solution to compare with the XFEM results. The bending equilibrium of the cross-section shown in Figure 12 can be written as

$$\int_A \sigma_x y \, dA + 2 \int f_s \frac{t}{2} \, dz = -M \tag{53}$$

where σ_x is the axial stress of the cross-section and f_s is the force induced on the beam surface due to the surface elastic constant S_{1111} ; $f_s = S_{1111} \varepsilon_{\max}$, where ε_{\max} is the maximum axial strain that occurs on the top and bottom surfaces. By applying the standard relationships $\sigma_x = E \varepsilon$ and

$\varepsilon = (y/y_{\max})\varepsilon_{\max}$ and substituting the result into (53) we find that:

$$\frac{2E}{t}\varepsilon_{\max} \int_A y^2 dA + S_{1111}tw\varepsilon_{\max} = -M \quad (54)$$

Knowing that $I = \int y^2 dA$, where I is section moment of inertia around axis z , one can write:

$$\varepsilon_{\max} = \frac{-M}{\frac{2EI}{t} + S_{1111}tw} \quad (55)$$

For the rectangular section shown in Figure 12, $I = \frac{1}{12}wt^3$; therefore, we can simplify Equation (55) to:

$$\varepsilon_{\max} = \frac{-M}{wt(\frac{1}{6}Et + S_{1111})} \quad (56)$$

while for ε we can write:

$$\varepsilon = \frac{-2My}{wt^2(\frac{1}{6}Et + S_{1111})} \quad (57)$$

If we now consider F and d as applied external force and its corresponding transverse deflection of the beam, the energy equilibrium can be written as

$$\delta W_{\text{ext}} = \delta F \cdot d = \delta W_b + \delta W_s + \delta W_{\text{sh}} \quad (58)$$

where δW_b , δW_s , and δW_{sh} are virtual internal energies corresponding with bending, surface, and shear deformation, respectively; and, δW_{ext} is virtual external work. The internal energies can be calculated as

$$\begin{aligned} \delta W_b &= \int_{\Omega} \sigma \cdot \delta \varepsilon d\Omega = \int_{\Omega} E \left(\frac{-2My}{wt^2(\frac{1}{6}Et + S_{1111})} \right) \left(\frac{-2\delta M y}{wt^2(\frac{1}{6}Et + S_{1111})} \right) d\Omega \\ &= \frac{4E}{w^2t^4(\frac{1}{6}Et + S_{1111})^2} \int M \delta M \left(\int y^2 dA \right) dx = \frac{E}{3wt(\frac{1}{6}Et + S_{1111})^2} \int M \cdot \delta M dx \end{aligned} \quad (59)$$

and

$$\begin{aligned} \delta W_s &= 2 \int f_s \cdot \delta \varepsilon_{\max} w dx = 2 \int S_{1111} \varepsilon_{\max} \cdot \delta \varepsilon_{\max} w dx \\ &= 2S_{1111}w \int \left(\frac{-M}{wt(\frac{1}{6}Et + S_{1111})} \right) \left(\frac{-\delta M}{wt(\frac{1}{6}Et + S_{1111})} \right) dx \\ &= \frac{2S_{1111}}{wt^2(\frac{1}{6}Et + S_{1111})^2} \int M \cdot \delta M dx \end{aligned} \quad (60)$$

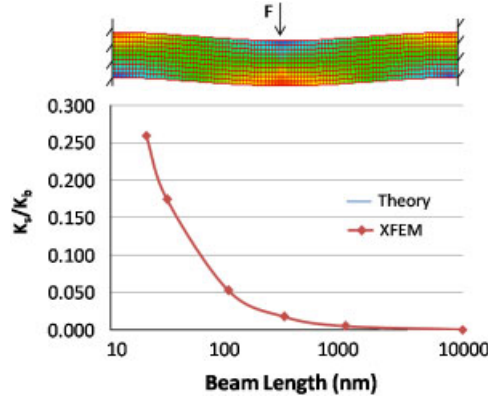


Figure 13. Comparison between XFEM and analytical solution for surface effects on the size-dependence of the transverse stiffness of a fixed-fixed nanobeam with a fixed aspect ratio of 10.

In Equation (59) we used $\int y^2 dA = wt^3/12$ as the moment of inertia for a rectangular cross-section. For a rectangular section with shear force V , shear modulus G and the Poisson ratio ν :

$$\delta W_{sh} = \frac{6}{5} \int \frac{V \cdot \delta V}{GA} dx = \frac{6}{5} \int \frac{2(1+\nu)V \cdot \delta V}{EA} dx \tag{61}$$

where A is the beam cross-sectional area. Combining Equations (58), (59), (60) and (61) and dividing by δF we can write:

$$d = \frac{2}{wt^2(\frac{1}{6}Et + S_{1111})} \int M \frac{\partial M}{\partial F} dx + \frac{12(1+\nu)}{5EA} \int V \frac{\partial V}{\partial F} dx \tag{62}$$

Following the theory of beams [37] for the fixed-fixed beam shown in Figure 12, we can derive that $M = FL((x/2L) - \frac{1}{8})$ and $V = F/2$ for $0 \leq x \leq L/2$. After further simplifying Equation (62) for a rectangular beam we find that:

$$K = \frac{F/w}{d} = \frac{1}{\frac{L^3}{96t^2(\frac{1}{6}Et + S_{1111})} + \frac{3L(1+\nu)}{5Et}} \tag{63}$$

where K is total transverse stiffness of the fixed-fixed beam under study. Figure 13 shows a comparison between the XFEM solution with the analytic solution in Equation (63) for fixed/fixed nanobeams with a constant aspect ratio of $L/t = 10$. There are two key trends to note. First, the agreement between the XFEM solution and the analytic solution is extremely good. Second, we observe the same trends for gold, i.e. a significant increase in effective Young’s modulus due to surface effects, that has been observed experimentally for fixed/fixed FCC metal nanowires both experimentally [35, 36] and theoretically by Yun and Park [25].

The effect of the combination of surface decohesion and surface elasticity on the overall mechanical response of a plate with an inclusion

The last example illustrates the combined effects of surface elasticity and surface decohesion, phenomena that can only be captured by considering both strong and weak discontinuities in the XFEM approximation. Referring to Figure 14(a), let us consider an elastic plate with a circular inclusion subjected to surface elasticity and interface decohesion. To describe surface elasticity, a weakly discontinuous enrichment is considered according to Equation (24), while the surface and bulk material properties [19] are given by $E = 3 \text{ GPa}$, $\nu = 0.3$, $S_{1111} = S_{2222} = 6.09 \text{ J/m}^2$, $S_{1122} = S_{2211} = 6.84 \text{ J/m}^2$, and $S_{1212} = -0.375 \text{ J/m}^2$, where E and ν are the bulk Young's modulus and the Poisson ratio, respectively. The dimensions of the plate are varying from $10 \text{ m} \times 10 \text{ m}$ to $10 \text{ nm} \times 10 \text{ nm}$ (Figure 14) in order to study the size effect on effective stiffness and the inclusion volume fraction is 0.2 for all simulations. To characterize matrix-inclusion decohesion, a linear cohesive law is also considered at the interface in the form given by Equation (12). We consider several interface stiffnesses K_t and K_n , ranging from zero to very large values ($1.0 \times 10^{15} \text{ Pa}$) and study the change of effective stiffness ($K_{\text{eff}} = \sigma_{yy} / \varepsilon_{yy}$), where σ_{yy} and ε_{yy} are the stress and strain in the vertical direction in the plate, respectively. For this, the deformation of the plate is prescribed as constant vertical displacement boundary conditions for the top and bottom edges and a fixed displacement on the left and right boundaries (Figure 14(a)). The deformed configuration of the plate for a weak cohesive stiffness is depicted in Figure 14, clearly showing the jump in displacement between points inside and outside the inclusion. The change in the normalized stiffness K_{eff} (with respect to the stiffness of the matrix material) with interface cohesion and plate dimension as computed with our XFEM formulation is then depicted in Figure 15. As expected, Figure 15 shows a rise of normalized effective stiffness with interface cohesive stiffness. The increase in effective stiffness occurs up to interface cohesive stiffnesses of about $K_n = K_t = 10 \text{ GPa}$ and is followed by a plateau as the interface decohesion becomes negligible compared with the plate deformation. Figure 15 also shows the strong size effect arising from surface elasticity applied on the inclusion as the plate dimension approaches nanometer dimensions. However, as cohesive stiffness decreases, the inclusion properties have a reduced effect on the effective properties of the plate. As a result, strong size effects are observed in the case of strong interface cohesion while when no cohesion is present ($K_n = K_t = 0$), no size effects are observed. This example therefore illustrates how a combination of weak and strong discontinuities is necessary to capture the interactions between surface elasticity and surface decohesion at the nano-scale.

CONCLUSIONS

We have introduced an XFEM/level set framework for the study of small deformation elastic behavior of nano-structures that possesses the following features:

- Owing to its continuum mechanics underpinnings, the method is computationally tractable and may be used to study surface and interface effects on nanostructures that have length scales, i.e. 10–100 nm, that are significantly larger than those that can be studied using fully atomistic techniques.
- The geometry of the structure is entirely defined by level set functions that are defined independently from the finite element mesh. Simple, regular FEM meshes may thus be used regardless of the geometric complexity of the nanostructure. The geometry of the structure is

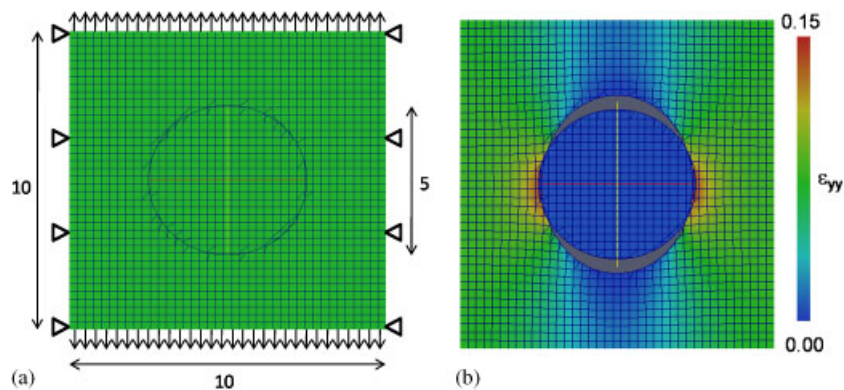


Figure 14. General outline of the plate under study: (a) undeformed and (b) deformed (zero interface cohesion). Sub-elements close to interface are used for plotting purposes only.

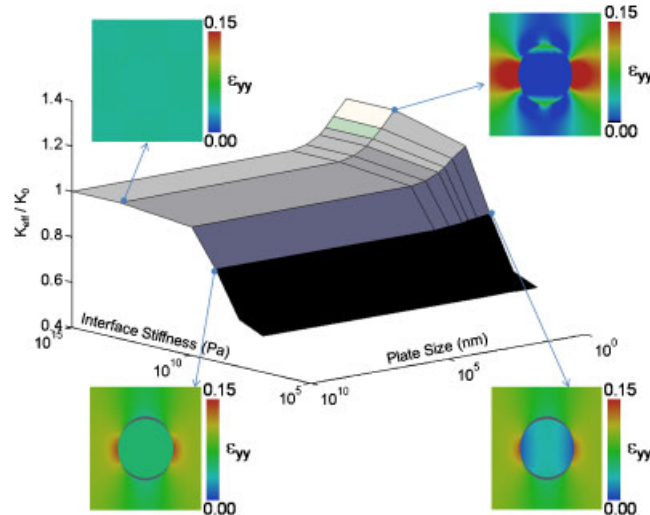


Figure 15. Changes of the plate effective stiffness with interface cohesion and scale.

entirely defined by level set functions that are defined independently from the finite element mesh. Simple, regular FEM meshes may thus be used regardless of the geometric complexity of the nanostructure. Another advantage of this method is that the external region that surrounds the area under study is deleted from the main problem solution by introducing a strong discontinuity. This method results in a well-conditioned global stiffness matrix by using a finite stiffness for the external region.

- The different elastic properties and constitutive response of nanoscale surfaces are described with a continuum description that naturally fits into the XFEM methodology. Thus, no special treatment is necessary to model jumps in stress, strain, and displacement arising due to free surfaces, interfaces, or interface decohesion.

- The method is able to describe complex material behavior in nano-composites such as plasticity or damage. It thus presents a useful tool for studying surface and interface effects on the deformation and fracture of nano-composite structures.

The developed methodology was verified against four numerical examples involving surface-stress-driven relaxation of a nanoplate and a multi-material bi-layer nanoplate, surface effects on the axial stiffness of a nanoplate, and surface effects on the bending stiffness of a nanobeam. In all cases, the XFEM/level set numerical results were in excellent agreement with the derived analytical solution. Furthermore, validation in the case of the surface-stress-driven relaxation of the gold nanoplate was performed against benchmark atomistic and multiscale SCB calculations. Finally, in the last example, a combination of weak and strong discontinuities was used to capture the interactions between surface decohesion and surface elasticity in a plate with an inclusion. The influence of surface properties and decohesion on the overall mechanical response of the composite plate could thus be assessed. Since surface elasticity was only associated with the inclusion, we observed a size dependence in the overall plate response when a finite cohesion between inclusion and matrix was considered. However, no size effects were observed when the interface cohesion vanished.

Future work will focus on incorporating the effects of plasticity and interface decohesion into the proposed framework [38–40], as well as detailed investigations into how surface effects impact the mechanical properties of nanomaterials.

ACKNOWLEDGEMENTS

FJV gratefully acknowledges NSF grant number CMMI-0900607 and HSP gratefully acknowledges NSF grant number CMMI-0750395 in support of this research.

REFERENCES

1. Sharma P, Ganti S, Bhate N. Effect of surfaces on the size-dependent elastic state of nano-inhomogeneities. *Applied Physics Letters* 2003; **82**(4):535–537.
2. Diao J, Gall K, Dunn ML. Surface stress driven reorientation of gold nanowires. *Physical Review B* 2004; **70**:075413.
3. Chen T *et al.* Size-dependent elastic properties of unidirectional nano-composites with interface stresses. *Acta Mechanica* 2007; **188**:39–54.
4. Cammarata RC. Surface and interface stress effects in thin films. *Progress in Surface Science* 1994; **46**(1):1–38.
5. Shenoy VB. Atomistic calculations of elastic properties of metallic FCC crystal surfaces. *Physical Review B* 2005; **71**:094104.
6. Mi C, Jun S, Kouris DA, Kim SY. Atomistic calculations of interface elastic properties in noncoherent metallic bilayers. *Physical Review B* 2008; **77**:075425.
7. Park HS, Klein PA. Surface Cauchy–Born analysis of surface stress effects on metallic nanowires. *Physical Review B* 2007; **75**:085408.
8. Park HS, Cai W, Espinosa HD, Huang H. Mechanics of crystalline nanowires. *MRS Bulletin* 2009; **34**(3):178–183.
9. Gurtin ME, Murdoch A. A continuum theory of elastic material surfaces. *Archives of Rational Mechanics and Analysis* 1975; **57**:291–323.
10. Yang P. The chemistry and physics of semiconductor nanowires. *MRS Bulletin* 2005; **30**(2):85–91.
11. Streitz FH, Cammarata RC, Sieradzki K. Surface-stress effects on elastic properties. I. Thin metal films. *Physical Review B* 1994; **49**(15):10699–10706.
12. Miller RE, Shenoy VB. Size-dependent elastic properties of nanosized structural elements. *Nanotechnology* 2000; **11**:139–147.
13. He LH, Lim CW, Wu BS. A continuum model for size-dependent deformation of elastic films of nano-scale thickness. *International Journal of Solids and Structures* 2004; **41**:847–857.

14. Sun CT, Zhang H. Size-dependent elastic moduli of platelike nanomaterials. *Journal of Applied Physics* 2003; **92**(2):1212–1218.
15. Dingreville R, Qu J, Cherkaoui M. Surface free energy and its effect on the elastic behavior of nano-sized particles, wires and films. *Journal of the Mechanics and Physics of Solids* 2005; **53**:1827–1854.
16. Wei G, Shouwen Y, Ganyun H. Finite element characterization of the size-dependent mechanical behaviour in nanosystems. *Nanotechnology* 2006; **17**:1118–1122.
17. She H, Wang B. A geometrically nonlinear finite element model of nanomaterials with consideration of surface effects. *Finite Elements in Analysis and Design* 2009; **45**:463–467.
18. He J, Lilley CM. The finite element absolute nodal coordinate formulation incorporated with surface stress effect to model elastic bending nanowires in large deformation. *Computational Mechanics* 2009; **44**(3):395–403.
19. Yvonnet J, Quang HL, He QC. An XFEM/level set approach to modelling surface/interface effects and to computing the size-dependent effective properties of nanocomposites. *Computational Mechanics* 2008; **42**: 119–131.
20. Park HS, Klein PA, Wagner GJ. A surface Cauchy–Born model for nanoscale materials. *International Journal for Numerical Methods in Engineering* 2006; **68**:1072–1095.
21. Park HS, Klein PA. A surface Cauchy–Born model for silicon nanostructures. *Computer Methods in Applied Mechanics and Engineering* 2008; **197**:3249–3260.
22. Park HS, Klein PA. Surface stress effects on the resonant properties of metal nanowires: the importance of finite deformation kinematics and the impact of the residual surface stress. *Journal of the Mechanics and Physics of Solids* 2008; **56**:3144–3166.
23. Park HS. Surface stress effects on the resonant properties of silicon nanowires. *Journal of Applied Physics* 2008; **103**:123504.
24. Park HS. Quantifying the size-dependent effect of the residual surface stress on the resonant frequencies of silicon nanowires if finite deformation kinematics are considered. *Nanotechnology* 2009; **20**:115701.
25. Yun G, Park HS. Surface stress effects on the bending properties of fcc metal nanowires. *Physical Review B* 2009; **79**:195421.
26. Gurtin ME. A general theory of curved deformable interfaces in solids at equilibrium. *Philosophical Magazine A* 1998; **78**(5):1093–1109.
27. Belytschko T, Liu WK, Moran B. *Nonlinear Finite Elements for Continua and Structures*. Wiley: New York, 2006.
28. Dolbow J, Moes N, Belytschko T. An extended finite element method for modeling crack growth with frictional contact. *Computer Methods in Applied Mechanics and Engineering* 2001; **190**(51–52):6825–6846.
29. Hettich T, Hund A, Ramm E. Modeling of failure in composites by x-fem and level sets within a multiscale framework. *Computer Methods in Applied Mechanics and Engineering* 2008; **197**:414–424.
30. Belytschko T, Parimi C, Moes N, Sukumar N, Usui S. Structured extended finite element methods for solids defined by implicit surfaces. *International Journal for Numerical Methods in Engineering* 2003; **56**(4):609–635.
31. Belytschko T, Gracie R. On xfem applications to dislocations and interfaces. *International Journal of Plasticity* 2007; **23**(10–11):1721–1738.
32. Moes N, Cloirec M, Cartraud P, Remacle JF. A computational approach to handle complex microstructure geometries. *Computer Methods in Applied Mechanics and Engineering* 2003; **192**:3163–3177.
33. Mohammadi S. *Extended Finite Element Method*. Blackwell: Oxford, 2008.
34. Dolbow J, Belytschko T. Finite element method for crack growth without remeshing. *International Journal for Numerical Methods in Engineering* 1999; **46**(1):131–150.
35. Jing GY, Duan HL, Sun XM, Zhang ZS, Xu J, Li YD, Wang JX, Yu DP. Surface effects on elastic properties of silver nanowires: contact atomic-force microscopy. *Physical Review B* 2006; **73**:235409.
36. Cuenot S, Frétiigny C, Demoustier-Champagne S, Nysten B. Surface tension effect on the mechanical properties of nanomaterials measured by atomic force microscopy. *Physical Review B* 2004; **69**:165–410.
37. Hibbeler R. *Structural Analysis*. Pearson, 2006.
38. Vernerey FJ *et al.* The 3-d computational modeling of shear-dominated ductile failure in steel. *Journal of the Minerals, Metals and Materials Society* 2006; **58**(12):45–51.
39. Vernerey FJ, Liu W, Moran B. Multi-scale micromorphic theory for hierarchical materials. *Journal of the Mechanics and Physics of Solids* 2007; **57**(12):2603–2651.
40. Vernerey FJ *et al.* A micromorphic model for the multiple scale failure of heterogeneous materials. *Journal of the Mechanics and Physics of Solids* 2007; **56**(4):1320–1347.